J Intell Robot Syst (2006) 46: 59–72
DOI 10.1007/s10846-006-9044-6

A New Approach to the Architecture Optimization of a General 3-PUU Translational Parallel Manipulator

Yangmin Li · Qingsong Xu

Received: 8 October 2004 / Accepted: 2 May 2006 /
Published online: 7 July 2006

Abstract This paper presents a new approach to the architecture optimization of a general 3-PUU translational parallel manipulator (TPM) based on the performance of a weighted sum of global dexterity index and a new performance index-space utility ratio (SUR). Both the inverse kinematics and forward kinematics solutions are derived in closed form, and the Jacobian matrix is derived analytically. The manipulator workspace is generated by a numerical searching method with the physical constraints taken into consideration. Simulation results illustrate clearly the necessity to introduce a mixed performance index using space utility ratio for architectural optimization of the manipulator, and the optimization procedure is carried out with the goal of reaching a compromise between the two indices. The analytical results are helpful in designing a general 3-PUU TPM, and the proposed design methodology can also be applied to architectural optimization for other types of parallel manipulators.

Key words dexterity · kinematics · optimal design · translational parallel manipulator · workspace

1. Introduction

Parallel mechanical architectures are first introduced in tire testing by Gough, and later are used by Stewart as motion simulators because of their unique advantages over serial mechanism. A parallel manipulator typically consists of a moving platform that is connected to a fixed base by several kinematic chains in parallel. A rather exhaustive enumeration of parallel robots with mechanical architectures and

Y. Li (✉) · Q. Xu
Department of Electromechanical Engineering, Faculty of Science and Technology,
University of Macau, Av. Padre Tomás Pereira S.J., Taipa, Macao S. A. R.,
People's Republic of China
e-mail: ymli@umac.mo

their versatile applications are described in [14]. A general six-degree-of-freedom (6-DOF) parallel manipulator has many advantages in terms of high accuracy, velocity, stiffness, and load carrying capability. However, six DOF is not always needed in many situations. In recent years, parallel manipulators with less than six DOF, which maintain the inherent advantages of parallel mechanisms and possess several other advantages such as reduction of the total cost of the device in manufactures and operations, are attracting attentions of various researchers. Many 3-DOF parallel manipulators have been designed and investigated for relevant applications, such as the famous DELTA robot with three translational DOF [2] whose concept then has been realized in many different configurations [11, 15, 22], Y-Star like and Orthoglide parallel robots with pure translational motions [1, 8], spherical 3-DOF manipulators with pure rotational DOF [6, 23], and 3-RPS and 3-PRS parallel mechanisms with combined translational and rotary motions [9, 12], etc.

Among them, translational parallel manipulators (TPMs) have potential wide applications where a pure translational motion is needed in cases of a motion simulator, a positioning tool of an assembly line, and others. Optimization methodologies have long been applied to mechanism design and a number of different optimization criteria for robot manipulators have been proposed. For any design problem, there will potentially be many objectives that cannot all be satisfied simultaneously. Probably this is the reason why most proposed optimal design procedures are focused only on the optimization of one main characteristics of the manipulator, such as dexterity [7], kinematic isotropy [4], and workspace [13], etc. However, specifying only a single objective may not yield an acceptable design. Unfortunately, only a few literatures involve the optimization problem by considering several criteria simultaneously [18, 19].

Compared with their serial counterparts, parallel manipulators suffer a main disadvantage of relatively small workspace. Thus it is natural to optimize the architectural parameters of a parallel manipulator to achieve a maximum total workspace volume. However, a manipulator designed for such objective may not be the optimal design for practical applications. As indicated in [17], it is possible that a parallel manipulator that is optimized for total workspace will result in a manipulator with undesirable kinematic characteristics such as poor dexterity. The dexterity of a manipulator can be thought as the ability of the manipulator to arbitrarily change its position and orientation, or apply forces and torques in arbitrary directions. For many applications, the manipulator is preferred to be designed with emphasis on dexterity together with a proper workspace size rather than on total workspace volume only.

In the literatures, different indices of manipulator dexterity are given. One of the frequently used indices is called kinematic manipulability that is defined by Yoshikawa [24] as the absolute value of determinant of the Jacobian. Since Jacobian (**J**) is configuration dependent, manipulability is a local performance measure. Another usually used index is the condition number of Jacobian matrix recommended by Salisbury and Craig [16]. It measures the degree of ill-conditioning of the Jacobian matrix, i.e., nearness of the singularity, and it is also a local measure of manipulator dexterity. A global dexterity index (GDI) is given by Gosselin and Angeles [7] in the form of

$$GDI = \frac{\int_V \left(\frac{1}{\kappa}\right) dV}{V}, \tag{1}$$

where V is the total workspace volume and κ denotes the condition number of the Jacobian. This global dexterity index represents the uniformity of manipulability over the entire workspace other than the dexterity at certain configuration, and is adopted in this paper since it possesses several favorable characteristics. For example, it is normalized by the workspace size and therefore gives a measure of kinematic performance independent of the differing workspace volume of design candidates. Furthermore, the reciprocal of condition number is bounded between 0 and 1, and is more convenient to handle than κ, which tends to infinity at singularities; hence, during numerical integration, the number of sample points near singularities has a reduced impact on the result since $1/\kappa$ approaches zero at those points.

Additionally, the space utility ratio (SUR) index is introduced in this paper to penalize designs in case of possessing large physical size yet producing relatively small workspace. The concept of space utility ratio is termed as space utilization to measure the ratio of cross-section size of workspace to the size of the robot that is estimated by area of the bonding box enclosing the robot's structure and workspace in the cross-section [18]. Alternatively, we define space utility ratio as the ratio of entire workspace volume to physical size of the robot that is taken as the product of area of the fixed platform and the maximum reach of the moving platform in the z-axis direction.

The 3-PUU architecture parallel manipulators are already well known in the mechanism community, and several 3-PUU TPMs have been designed and analyzed separately [5, 21]. Although these manipulators have different methods in actuators arrangement, they still can be considered as the same type of mechanism since they can be resolved using the same kinematics technique. We propose a general 3-PUU TPM in this paper, where the term 'general' describes the arbitrary values of the actuators layout angle of the manipulator which is adjustable. In this communication, the architectural optimization for a general 3-PUU TPM is developed by a new approach which is based on the performance that is a weighted sum of global dexterity index and a new performance index, space utility ratio. The optimization is performed with the goal of reaching a compromise between dexterity and workspace size of the manipulator, since these two important indices usually can not be optimized at the same time as illustrated by the simulation results.

2. Description of a General 3-PUU TPM

The schematic diagram of a general 3-PUU TPM is represented in Figure 1. It consists of a moving platform, a fixed base, and three limbs of identical kinematic structure. Each limb connects the fixed base to the moving platform by a prismatic (P) joint followed by two universal (U) joints in sequence, where the P joint is driven by a linear actuator.

Since each U joint consists of two intersecting revolute joints, each limb is kinematically equivalent to a PRRRR chain. It is shown that in order to keep the moving platform from changing its orientation, it is sufficient for the four revolute joint axes within the same limb to satisfy some certain geometric conditions [3, 20]. That is, the first revolute joint axis is parallel to the last revolute joint axis; the two intermediate joint axes are parallel to one another. Since the geometric conditions stated above do not require the U joint axes to intersect at a point, any 3-PRRRR

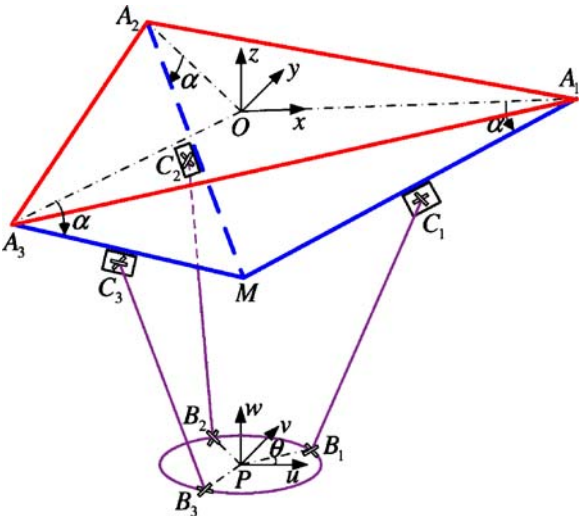

Figure 1 Schematic of a general 3-PUU TPM.

parallel manipulator whose revolute joint axes satisfy the above conditions will result in a manipulator with a pure translational motion.

One typical kinematic chain of a general 3-PUU TPM is shown in Figure 2. For the purpose of analysis, as represented in Figure 1 and Figure 2, we assign a fixed Cartesian coordinate system $O\{x, y, z\}$ at the centered point O of the fixed base platform $\Delta A_1 A_2 A_3$, and a moving Cartesian frame $P\{u, v, w\}$ on the moving platform at the centered point P of triangle $\Delta B_1 B_2 B_3$. For simplification and without the loss of generality, let the x-axis and u-axis be parallel to one another, and the x-axis direct along $\overrightarrow{OA_1}$. Vector $\overrightarrow{OA_i}$ is not necessarily parallel to vector $\overrightarrow{PB_i}$, and the angle between $\overrightarrow{PB_i}$ and $\overrightarrow{OA_i}$ $(i = 1, 2, 3)$ is defined as the twist angle θ, i.e., the angle between the moving platform and the fixed base. The three rails $D_i E_i (\ i = 1, 2, 3)$

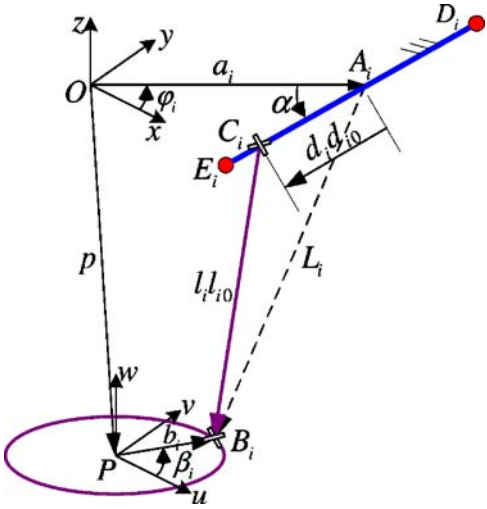

Figure 2 Geometry of one typical kinematic chain.

intersect each other at point M, and intersect the x–y plane at points A_1, A_2, and A_3 that lie on a circle of radius a. The three links C_iB_i $(i = 1, 2, 3)$ with the length of l intersect the u–v plane at points B_1, B_2, and B_3 which lie on a circle of radius b. The sliders of the P joints are restricted to move along the rails between D_i and E_i. Angle α is measured from the fixed base to rails D_iE_i and is defined as the actuators layout angle. Angle φ_i is measured from the x-axis to vector $\overrightarrow{OA_i}$ in the fixed frame, and angle β_i is measured from the u-axis to vector $\overrightarrow{PB_i}$ in the moving frame. For simplicity, we assign that

$$\varphi_i = (i-1) \times 120^\circ, \tag{2}$$

$$\beta_i = \theta + (i-1) \times 120^\circ, \tag{3}$$

for $i = 1$, 2, and 3. As illustrated in Section 5, this assignment also results in a symmetric workspace of the manipulator.

3. Kinematics Analysis

3.1. Inverse Kinematics Modeling

The inverse kinematics problem resolves the actuated variables from a given moving platform position. As shown in Figure 2, the position vectors of points A_i and B_i with respect to frames O and P, respectively, can be written as

$$^O\mathbf{a}_i = [ac\varphi_i \quad as\varphi_i \quad 0]^T, \tag{4}$$

$$^P\mathbf{b}_i = [bc\beta_i \quad bs\beta_i \quad 0]^T, \tag{5}$$

where c stands for cosine, s stands for sine, and a leading superscript indicates the coordinate frame that a vector is expressed. For brevity, the leading superscript will be omitted whenever the coordinate frame is the fixed base frame, e.g. $^O\mathbf{a}_i = \mathbf{a}_i$. Generally, the position and orientation of the moving platform with respect to the fixed frame can be described by a position vector, $\mathbf{p} = \overrightarrow{OP}$, and a 3×3 rotation matrix $^O\mathbf{R}_P$. However, since the moving platform possesses only a translational motion, $^O\mathbf{R}_P$ becomes an identity matrix. Then, we have

$$^P\mathbf{b}_i = \mathbf{b}_i\,. \tag{6}$$

Referring to Figure 2, a vector-loop equation can be written for the i-th limb as follows:

$$l\,\mathbf{l}_{i0} = \mathbf{L}_i - d_i\mathbf{d}_{i0}\,, \tag{7}$$

with

$$\mathbf{L}_i = \mathbf{p} + \mathbf{b}_i - \mathbf{a}_i\,, \tag{8}$$

where $\mathbf{l}_{i0}$ is the unit vector along $\overrightarrow{C_iB_i}$; d_i represents the linear displacement of the i-th actuator; $\mathbf{d}_{i0}$ is the corresponding unit vector pointing along rail D_iE_i, which can be expressed as

$$\mathbf{d}_{i0} = [-c\alpha c\varphi_i \quad -c\alpha s\varphi_i \quad -s\alpha]^T\,. \tag{9}$$

Dot-multiplying Equation (7) with itself and rearranging the terms, yields

$$d_i^2 - 2d_i\mathbf{d}_{i0}^T\mathbf{L}_i + \mathbf{L}_i^T\mathbf{L}_i - l^2 = 0\,. \tag{10}$$

Solving Equation (10), the inverse kinematics solutions can be derived as

$$d_i = \mathbf{d}_{i0}^T\mathbf{L}_i \pm \sqrt{(\mathbf{d}_{i0}^T\mathbf{L}_i)^2 - \mathbf{L}_i^T\mathbf{L}_i + l^2}\,, \quad i = 1,\ 2,\ 3. \tag{11}$$

We can see that there exist two solutions for each actuator, hence there are total of eight possible solutions for a given moving platform position. In this paper, only the negative square root is selected to yield a solution where the three legs are inclined inward from top to bottom.

3.2. Forward Kinematics Modeling

Given a set of the actuated inputs, the position of the moving platform is resolved by the forward kinematics. From Equations (7) and (8), we can get

$$l\,\mathbf{l}_{i0} = \mathbf{p} - \mathbf{e}_i\,, \tag{12}$$

where

$$\mathbf{e}_i = \mathbf{a}_i + d_i\mathbf{d}_{i0} - \mathbf{b}_i\,. \tag{13}$$

Dot-multiplying Equation (12) with itself and rearranging the items, yields

$$\mathbf{p}^T\mathbf{p} - 2\mathbf{p}^T\mathbf{e}_i + \mathbf{e}_i^T\mathbf{e}_i = l^2\,. \tag{14}$$

Writing Equation (14) three times, once for taking $i = 1$, 2 and 3, respectively, yields three equations in $\mathbf{p}$. Each equation represents a sphere of radius l with its center located at the end point N_i of a vector defined by point O and $\mathbf{e}_i$. The intersection of these spheres yields the solutions to the forward kinematics problem. In general, there are two solutions since the intersection of two spheres forms a circle which will generally intersect the third sphere in two points. The following four cases are possible:

- Two solutions. The two solutions are realized at the intersection of three spheres.
- One solution. Two of the spheres may be tangent to each other, which results in a double root if the point of contact lies on the third sphere.
- Infinite solutions. This is the case when two or three of the three spheres coincide, i.e., they are of equal radii and concentric.
- No solution. The three spheres do not intersect in real space.

Subtracting Equation (14) for i=1 from Equation (14) for i=2 and 3, respectively, yields

$$\mathbf{p}^T(\mathbf{e}_2 - \mathbf{e}_1) - h_2 = 0\,, \tag{15}$$

$$\mathbf{p}^T(\mathbf{e}_3 - \mathbf{e}_1) - h_3 = 0\,, \tag{16}$$

where $h_2 = (\mathbf{e}_2^T\mathbf{e}_2 - \mathbf{e}_1^T\mathbf{e}_1)/2$ and $h_3 = (\mathbf{e}_3^T\mathbf{e}_3 - \mathbf{e}_1^T\mathbf{e}_1)/2$.

Equations (15) and (16) represent two linear functions in three unknowns of p_x, p_y and p_z, from which p_x and p_y can be expressed in terms of p_z as follows:

$$p_x = k_1 + p_z k_2 \,, \tag{17}$$

$$p_y = k_3 + p_z k_4 \,, \tag{18}$$

where $k_1 = S_1/S_{01}$, $k_2 = S_2/S_{01}$, $k_3 = S_3/S_{02}$, $k_4 = S_4/S_{02}$, with $S_1 = h_2(e_{3y} - e_{1y}) - h_3(e_{2y} - e_{1y})$, $S_2 = (e_{3z} - e_{1z})(e_{2y} - e_{1y}) - (e_{2z} - e_{1z})(e_{3y} - e_{1y})$, $S_{01} = (e_{2x} - e_{1x})(e_{3y} - e_{1y}) - (e_{3x} - e_{1x})(e_{2y} - e_{1y})$, $S_3 = h_2(e_{3x} - e_{1x}) - h_3(e_{2x} - e_{1x})$, $S_4 = (e_{3z} - e_{1z})(e_{2x} - e_{1x}) - (e_{2z} - e_{1z})(e_{3x} - e_{1x})$, $S_{02} = (e_{2y} - e_{1y})(e_{3x} - e_{1x}) - (e_{3y} - e_{1y})(e_{2x} - e_{1x})$.

Substituting Equations (17) and (18) into Equation (14) for i=1, yields

$$T_1 p_z^2 + 2T_2 p_z + T_3 = 0 \,, \tag{19}$$

where $T_1 = k_2^2 + k_4^2 + 1$, $T_2 = k_1 k_2 + k_3 k_4 - e_{1x} k_2 - e_{1y} k_4 - e_{1z}$, and $T_3 = k_1^2 + k_3^2 - 2e_{1x} k_1 - 2e_{1y} k_3 - l^2$. Solving Equation (19), yields

$$p_z = \frac{-T_2 \pm \sqrt{T_2^2 - T_1 T_3}}{T_1} \,. \tag{20}$$

Thus, Equations (17), (18), and (20) represent the solutions of forward kinematics. When there are two different real solutions, the two corresponding points form a mirror image of each other about the plane defined by the three sphere center points N_1, N_2, and N_3. Thus, one point is located below the actuators, and the other one above ($p_z > 0$). Only the point below the actuators with smaller p_z value is taken into consideration for practical applications, since the point above the actuators could only be obtained by reassembling the manipulator. And the unique feasible configuration is an important feature for real time control in robotic applications.

4. Jacobian Matrix Generation

Substituting Equation (8) into Equation (7) and differentiating it with respect to time, yields

$$\dot{d}_i \mathbf{d}_{i0} = \dot{\mathbf{x}} - l\,\omega_i \times \mathbf{l}_{i0} \,, \tag{21}$$

where ω_i denotes the angular velocity vector of link $C_i B_i$ with respect to the fixed frame, and $\dot{\mathbf{x}} = [\dot{p}_x \quad \dot{p}_y \quad \dot{p}_z]^T$ is the vector of linear velocity of the moving platform.

Dot-multiplying both sides of Equation (21) by $\mathbf{l}_{i0}$ yields

$$\mathbf{l}_{i0}^T \mathbf{d}_{i0} \dot{d}_i = \mathbf{l}_{i0}^T \dot{\mathbf{x}} \,. \tag{22}$$

Writing Equation (22) three times in terms of i=1, 2, and 3, three scalar equations can be obtained in matrix form as

$$\mathbf{J}_q \dot{\mathbf{q}} = \mathbf{J}_x \dot{\mathbf{x}} \,, \tag{23}$$

where

$$\mathbf{J}_q = \begin{bmatrix} \mathbf{l}_{10}^T \mathbf{d}_{10} & 0 & 0 \\ 0 & \mathbf{l}_{20}^T \mathbf{d}_{20} & 0 \\ 0 & 0 & \mathbf{l}_{30}^T \mathbf{d}_{30} \end{bmatrix}, \quad \mathbf{J}_x = \begin{bmatrix} \mathbf{l}_{10}^T \\ \mathbf{l}_{20}^T \\ \mathbf{l}_{30}^T \end{bmatrix},$$

and $\dot{\mathbf{q}} = [\dot{d}_1 \quad \dot{d}_2 \quad \dot{d}_3]^T$ is the vector of actuated joint rates. When the manipulator is away from the singularity, from Equation (23), we can obtain

$$\dot{\mathbf{q}} = \mathbf{J}\,\dot{\mathbf{x}}, \tag{24}$$

where

$$\mathbf{J} = \mathbf{J}_q^{-1}\mathbf{J}_x \tag{25}$$

is the 3×3 Jacobian matrix of a general 3-PUU TPM, which relates the output velocities to the actuated joint rates.

5. Workspace Generation

5.1. Physical Constraints

In the design of a general 3-PUU TPM, some physical constraints should be taken into consideration, such as the U joint cone angle limit and the actuator motion range. Here, we discuss the constraints introduced by cone angle limit of the U joints. Figure 3 describes the top view of a general 3-PUU TPM at the home position. And the two cone angle limits (η) of one U joint are represented in Figure 4. For i-th PUU kinematics chain, as illustrated in Figure 5(a), the two outer revolute joint axes which are parallel with each other are arranged to be perpendicular to the direction of link $C_i B_i$ and lie in plane 1 which is parallel to the z-axis, and the two inner revolute joint axes which are parallel with each other are arranged to be perpendicular to vector $\overrightarrow{C_i B_i}$ and lie in plane 2 which is perpendicular to plane 1.

For universal joint C_i, the cone angle of the outer revolute joint is defined as the angle γ_{i1} between link $C_i B_i$ and plane 1, and cone angle of the inner revolute joint is

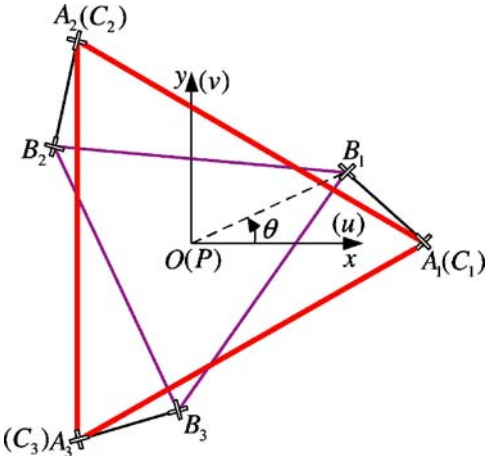

Figure 3 Top view of the TPM at home position.

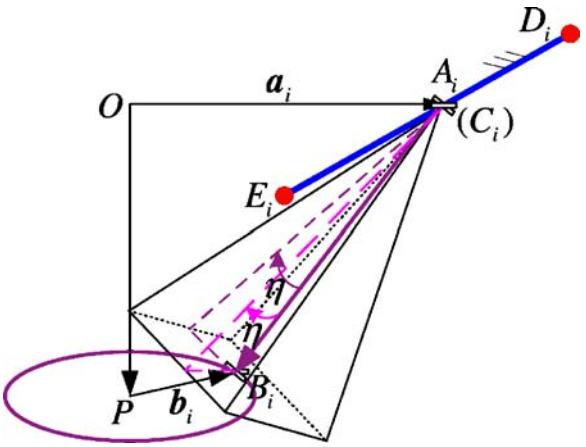

Figure 4 Cone angle limits of a universal joint.

defined as the angle γ_{i2} between link $C_i B_i$ and plane 2, as described in Figure 5(b), respectively. Considering the relationship between normal vectors of the planes and direction vector of the link, the two cone angles can be solved as follows.

$$\gamma_{i1} = \sin^{-1}\left(\frac{\mathbf{n}_{i1}^T \mathbf{l}_{i0}}{|\mathbf{n}_{i1}|}\right), \tag{26}$$

$$\gamma_{i2} = \sin^{-1}\left(\frac{\mathbf{n}_{i2}^T \mathbf{l}_{i0}}{|\mathbf{n}_{i2}|}\right), \tag{27}$$

where $\mathbf{n}_{i1}$ and $\mathbf{n}_{i2}$ denote the normal vectors of plane 1 and plane 2, respectively. We assume that the cone angle limits of the U joints are $\eta = 20°$, i.e., $-20° \leq \gamma_{i1} \leq 20°$, and $-20° \leq \gamma_{i2} \leq 20°$.

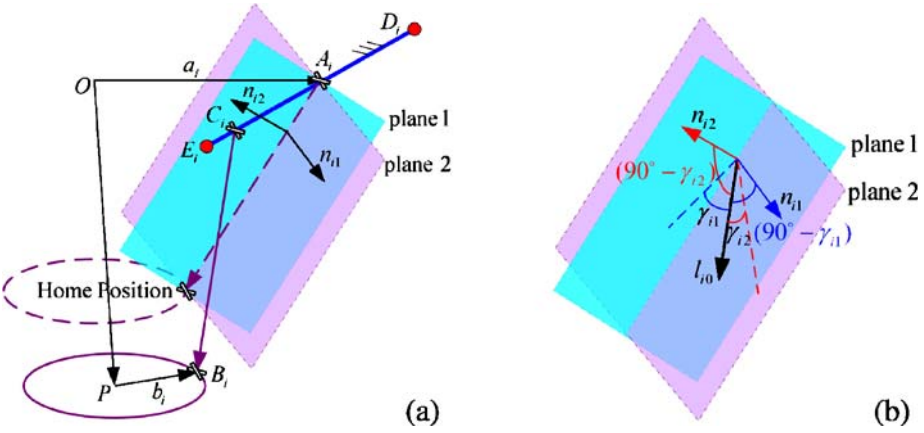

Figure 5 Calculating the cone angles for a universal joint. **a** Normal vectors of plane 1 and plane 2. **b** Cone angles of one universal joint.

5.2. Algorithms

By changing the coordinates of the three P joints within their motion range and resorting to solutions of the forward kinematics problem, the workspace shape can be easily expressed in 3-D space by a series of dots. It can be observed that there exist no any holes within the workspace, i.e., the cross-section of workspace is consecutive at every height. This allows the use of a numerical search method in cylindrical coordinates by slicing the workspace into a series of sub-workspace [10], and the boundary of each sub-workspace is successively determined through the inverse kinematics solutions along with the physical constraints taken into consideration. The total workspace volume is approximately calculated as the sum of a series of sub-workspace.

6. Architecture Optimization

6.1. Performance Index

The objective function for maximization is defined as a mixed performance index which is a weighted sum of global dexterity index (GDI) η_d and space utility ratio (SUR) index η_s, i.e.,

$$\eta = w_d\,\eta_d + (1 - w_d)\eta_s \tag{28}$$

$$= w_d \left(\frac{1}{V} \int_V \frac{1}{\kappa}\, dV \right) + (1 - w_d)\frac{V}{V^*}, \tag{29}$$

where the weight parameter w_d $(0 \le w_d \le 1)$ describes the proportion of GDI in the mixed index, and V^* represents the robot size which is evaluated by the product of area of the fixed platform and the maximum reach of the moving platform in the z direction.

The condition number of Jacobian matrix $\mathbf{J}$ can be defined as

$$\kappa = \| \mathbf{J} \| \, \| \mathbf{J}^{-1} \|, \tag{30}$$

where $\| \bullet \|$ denotes the two-norm of the matrix.

6.2. Design Variables

The architectural parameters of a general 3-PUU TPM involve size of the fixed base platform (a), size of the moving platform (b), length of legs (l), twist angle (θ), and actuators layout angle (α). To achieve a symmetric workspace, we assume that $\theta = 0^\circ$ in this paper. In order to perform the optimization independent of the dimension of each design candidate, the first three design variables are scaled by Δd, i.e., the motion range of P joints. Thus, the design variables become $\frac{a}{\Delta d}$, $\frac{b}{\Delta d}$, $\frac{l}{\Delta d}$, and α.

6.3. Computational Issues

The limits selected for the design variables are as follows: $0.5 \le \frac{a}{\Delta d} \le 4.0$, $0.5 \le \frac{b}{\Delta d} \le 4.0$, $1.0 \le \frac{l}{\Delta d} \le 4.0$, and $0^\circ \le \alpha \le 105^\circ$. To enhance the stiffness of the manipulator,

Table I Numerical results of the optimization

w_d	$a/\Delta d$	$b/\Delta d$	$l/\Delta d$	α (°)
0	1.5	0.5	3.0	60
0.5	1.5	0.5	1.5	45
1.0	3.0	0.5	3.0	60

the radius of the moving platform is selected as a smaller value than that of the fixed base so that the three legs are inclined inward from top to bottom. Since there exist no closed-form solutions for global dexterity index, the integral of the dexterity must be calculated numerically, which can be approximated by a discrete sum:

$$\eta_d \approx \frac{1}{N_w} \sum_{w \in V} \frac{1}{\kappa}, \tag{31}$$

where w is one of N_w points which are uniformly distributed over the entire workspace of the manipulator.

7. Optimization Results

The optimization was performed with various values of the weight parameter w_d in MATLAB environment, and the results for several values were presented in Table I. Let $\Delta d = 2$, the workspace of the manipulator with optimized parameters as presented in Table I in case of $w_d = 0.5$ is displayed in Figure 6, from which we can observe that the workspace is 120-degree symmetrical about the three actuator directions in vertical view, which can be divided into the upper, middle, and lower part. The upper and lower parts take on the triangular cross-section in shape, and the cross-section of the middle part looks like a hexagon.

With the varying of actuators layout angle, the results of optimized global dexterity index (GDI), space utility ratio (SUR) index, and maximum workspace volume are shown in Figures 7, 8 and 9, respectively, from which we can observe that the

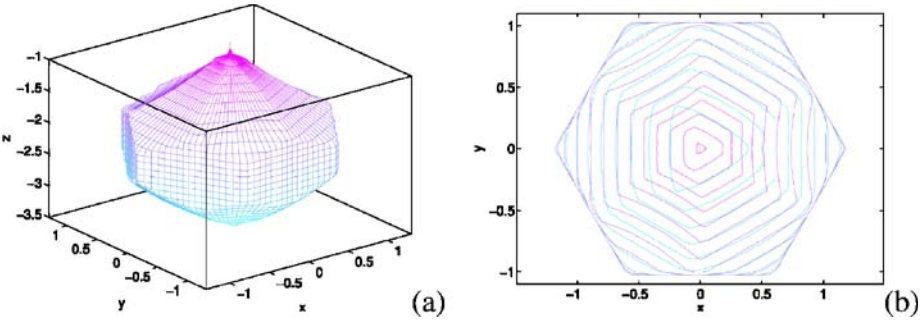

Figure 6 Workspace of a general 3-PUU TPM in case of $w_d = 0.5$. **a** *Three-dimensional view*. **b** *Top view*.

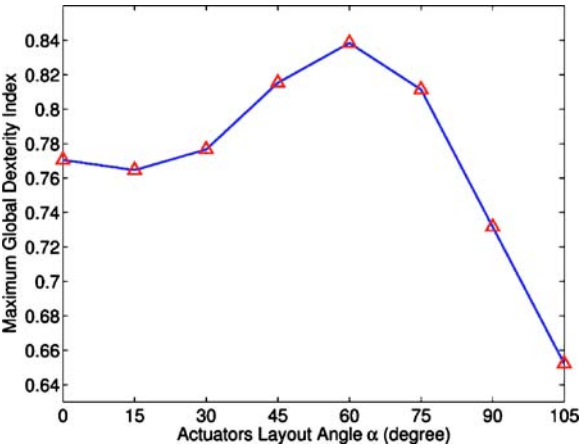

Figure 7 Maximum global dexterity index *versus* actuators layout angle.

optimization process with respect to different performance indices results in different sets of parameters of the manipulator.

Simulation results illustrate that when the manipulator is optimized for maximum total workspace volume only, the optimal parameters are $\frac{a}{\Delta d} = 3.0$, $\frac{b}{\Delta d} = 2.0$, $\frac{l}{\Delta d} = 4.0$, $\alpha = 75^\circ$, with the obtained maximum workspace volume $V_1 = 28.4819$, and the corresponding space utility ratio $\eta_{s1} = 0.0694$. Comparing these parameters with those optimized for maximum SUR index, i.e., $w_d = 0$, $\frac{a}{\Delta d} = 1.5$, $\frac{b}{\Delta d} = 0.5$, $\frac{l}{\Delta d} = 3.0$, $\alpha = 60^\circ$ as shown in Table I, and the corresponding workspace volume $V_2 = 16.3838$ and space utility ratio $\eta_{s2} = 0.2099$, allows the calculation of $\frac{V_1}{V_2} = 1.74$, and $\frac{\eta_{s2}}{\eta_{s1}} = 3.02$. It is clear that the optimized manipulator for maximum workspace volume possesses a comparatively large physical size yet gives relatively small workspace size.

Moreover, when the optimization is conducted to achieve maximum GDI only, i.e., $w_d = 1.0$, the results lead to a manipulator with the parameters as indicated in Table I, and with the GDI of $\eta_{d3} = 0.8384$ and the SUR of $\eta_{s3} = 0.0232$. Comparing

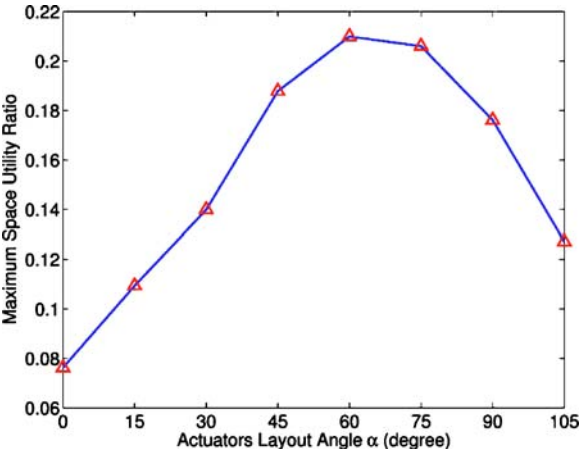

Figure 8 Maximum space utility ration *versus* actuators layout angle.

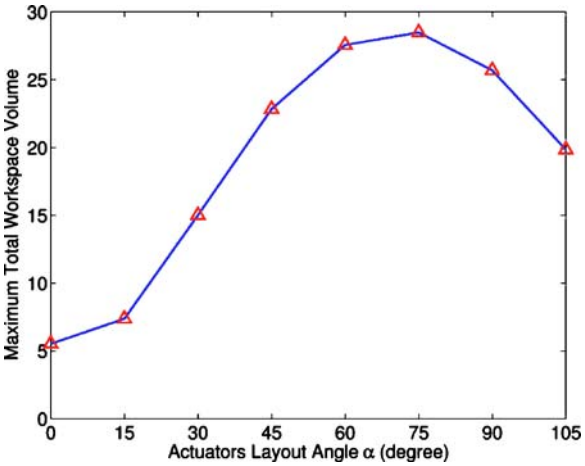

Figure 9 Maximum workspace volume *versus* actuators layout angle.

these values with those optimized for maximum SUR only, i.e. $w_d = 0$, $\eta_{d2} = 0.2316$, and $\eta_{s2} = 0.2099$, we can derive $\frac{\eta_{d3}}{\eta_{d2}} = 3.62$, and $\frac{\eta_{s2}}{\eta_{s3}} = 9.05$. That is, the optimization developed for maximum GDI results in a manipulator with small SUR, and *vice versa*.

The derived simulation results sufficiently show that it is necessary to introduce the aforementioned performance index, space utility ratio (SUR), and adopt a mixed performance index for architectural optimization of a general 3-PUU TPM by reaching a better compromise between dexterity and workspace size, which heavily depends on the specific objective.

8. Conclusions

The architecture optimization for a general 3-PUU TPM is performed in terms of a mixed performance index composed of both a weighted sum of global dexterity index over the entire workspace and a new performance index – space utility ratio defined as the ratio of total workspace volume to physical size of the manipulator. Space utility ratio (SUR) is a concept proposed to avoid the cases where the design candidates have large physical size yet produce relatively small workspace. The mixed performance index is adopted to overcome the often encountered problems, if a manipulator is optimized with emphasis only on dexterity characteristics usually it will result in a singularity-free workspace but with a relatively small SUR value. The architectural optimization developed for a general 3-PUU TPM is successfully implemented in MATLAB environment. And the simulation results provide a sound basis for optimization of the manipulator with selected weight parameters that are appropriated for different specific applications. Furthermore, the methodology presented here can also be applied for architectural optimization of other types of parallel manipulators.

Acknowledgments The authors appreciate the fund support from the research committee of University of Macau under grant no.: RG068/05-06S/LYM/FST and Macao Science and Technology Development Fund under grant no.: 069/2005/A.

References

1. Chablat, D., Wenger, P.: Architecture optimization of a 3-DOF translational parallel mechanism for machining applications, the Orthoglide. IEEE Trans. Robot. Autom. **19**(3), 403–410 (2003)
2. Clavel, R.: DELTA, a fast robot with parallel geometry. In: Proc. of 18th Int. Symp. Industrial Robots, Lausanne, pp. 91–100 (1988)
3. Di Gregorio, R. and Parenti-Castelli, V.: A translational 3-DOF parallel manipulator. In: Lenarcic, J., Husty, M.L. (eds.) Advances in Robot Kinematics: Analysis and Control, pp. 49–58 (1998)
4. Fattah, A., Hasan Ghasemi, A.M.: Isotropic design of spatial parallel manipulators. Int. J. Rob. Res. **21**(9), 811–824 (2002)
5. Giberti, H., Righettini, P., Tasora, A.: Design and experimental test of a pneumatic translational 3DOF parallel manipulator. In: Proc. of 10th Int. Work. Rob. in RAAD. Vienna, Austria (2001)
6. Gosselin, C., Angeles, J.: The optimum kinematic design of a spherical three-degree-of-freedom parallel manipulator. ASME J. Mech. Transm. Autom. Des. **111**(2), 202–207 (1989)
7. Gosselin, C., Angeles, J.: A global performance index for the kinematic optimization of robotic manipulators. ASME J. Mech. Des. **113**(3), 220–226 (1991)
8. Herve, J.M., Sparacino, F.: Star, a new concept in rbotics. In: Proc. of Advances in Robot Kinematics. Ferrara, Italy, pp. 176–183 (1992)
9. Lee, K.M., Arjunan, S.: A three-degrees-of-freedom micromotion in-parallel actuated manipulator. IEEE Trans. Robot. Autom. **7**(5), 634–641 (1991)
10. Li, Y., Xu, Q.: Kinematics and stiffness analysis for a general 3-PRS spatial parallel mechanism. In: Proc. of 15th CISM/IFToMM Symp. Robot Design, Dynamics and Control, Montreal, Canada (2004)
11. Li, Y., Xu, Q.: Dynamic analysis of a modified DELTA parallel robot for cardiopulmonary resuscitation. In: Proc. of IEEE/RSJ Int. Conf. on Intelligent Robots and Systems, Edmonton, Canada, pp. 3371–3376 (2005)
12. Li, Y., Xu, Q.: Kinematics and inverse dynamics analysis for a general 3-PRS spatial parallel mechanism. Robotica **23**(2), 219–229 (2005)
13. Merlet, J.-P.: Workspace-oriented methodology for designing a parallel manipulator. In: Proc. of IEEE Int. Conf. Robotics and Automation, Minneapolis, Minnesota, pp. 3726–3731 (1996)
14. Merlet, J.-P.: Parallel Robots. Kluwer, London (2000)
15. Miller, K.: Synthesis of a manipulator of the new UWA robot. In: Proc. of Australian Conf. on Robotics and Automation, Brisbane, Australian, pp. 228–233 (1999)
16. Salisbury, J., Craig, J.: Articulated hands: Force control and kinematic issues. Int. J. Rob. Res. **1**(1), 4–17 (1982)
17. Stamper, R.E., Tsai, L.W., Walsh, G. C.: Optimization of a three DOF translational platform for well-conditioned workspace. In: Proc. of IEEE Int. Conf. Robotics and Automation, Albuquerque, New Mexico, pp. 3250–3255 (1997)
18. Stock, M., Miller, K.: Optimal kinematic design of spatial parallel manipulators: Application to linear Delta robot. ASME J. Mech. Des. **125**(2), 292–301 (2003)
19. Stoughton, R.S., Arai, T.: A modified Stewart platform manipulator with improved dexterity. IEEE Trans. Robot. Autom. **9**(2), 166–173 (1993)
20. Tsai, L.W.: Kinematics of a three-DOF platform with three extensible limbs. In: Lenarcic, J., Parenti-Castelli, V. (eds.) Recent Advances in Robot Kinematics, pp. 401–410 (1996)
21. Tsai, L.W., Joshi, S.: Kinematics analysis of 3-DOF position mechanisms for use in hybrid kinematic machines. ASME J. Mech. Des. **124**(2), 245–253 (2002)
22. Tsai, L.W., Walsh, G.C., Stamper, R.E.: Kinematics of a novel three DOF translational platform. In: Proc. of IEEE Int. Conf. on Robotics and Automation, Minneapolis, Minnesota, pp. 3446–3451 (1996)
23. Vischer, P., Clavel, R.: Argos: A novel 3-DOF parallel wrist mechanism. Int. J. Rob. Res. **19**(1), 5–11 (2000)
24. Yoshikawa, T.: Manipulability of robotic mechanisms. Int. J. Rob. Res. **4**(2), 3–9 (1985)